Journal of Alloys and Compounds 898 (2022) 162916

Contents lists available at ScienceDirect

Journal of Alloys and Compounds

journal homepage: www.elsevier.com/locate/jalcom

Crystal growth, structure and thermal properties of anhydrous zinc carbonate ($ZnCO_3$)

Wen Liang[a,d,e,1,*], Jie Bai[c,1], Zengsheng Li[f], Yong Meng[a,d,e], Kaixiang Liu[a], Lin Li[b,g,**]

[a] College of Material Science and Engineering, Guizhou Minzu University, Guiyang 550025, China
[b] State Key Laboratory of Geological Processes and Mineral Resources, China University of Geosciences, Beijing 100083, China
[c] Analysis and test center, Guangdong University of Technology, Guangzhou 510075, China
[d] University of Chinese Academy of Sciences, Beijing 100049, China
[e] Institute of Geochemistry, Chinese Academy of Sciences, Guiyang 550081, China
[f] Shandong Geological Sciences Institute, Jinan 250013, China
[g] Institute of Science Research, China University of Geosciences, Beijing 100083, China

ARTICLE INFO

Article history:
Received 20 August 2021
Received in revised form 19 November 2021
Accepted 21 November 2021
Available online 30 November 2021

Keywords:
Anhydrous zinc carbonate ($ZnCO_3$)
Flame retardant
High pressure synthesis
Single crystal growth
Crystal structure
Thermal properties

ABSTRACT

Carbonate materials have been increasingly favoured in terms of the development of flame retardants because of the eternal subject of inorganic carbon sequestration. In this regard, anhydrous zinc carbonate ($ZnCO_3$) has been deemed as suitable candidate thanks to its excellent flame retardancy compared to traditional hydroxid flame retardant. However, the single crystals growth, accurate characterizations of structural and thermal properties are still not entirely clear from previous studies. With this in mind, $ZnCO_3$ single crystals were synthesized under high-pressure-temperature conditions (high P-T; 3 GPa and 973 K). The crystal structure of impurity-free $ZnCO_3$ was determined by means of single crystal X-ray diffraction (XRD). The symmetry was identified as $R\bar{3}c$, while the unit cell parameters were a= 4.6463(3) Å and c= 15.0015(11) Å with a final R value of 0.0229. The quantitative analyses of Raman spectrum and infrared absorption indicate that the as-synthesized $ZnCO_3$ is anhydrous phase. Using Thermogravimetric (TG) / Differential Scanning Calorimeter (DSC) measurements, $ZnCO_3$ was decomposed in the temperature range of 593–773 K, whereas the heat capacity and the endothermic peak were determined. According to the single crystal XRD from 150 K to 383 K, the thermal expansion coefficients were quantified as $\alpha_a = 7.90 \times 10^{-6}$ K^{-1} and $\alpha_c = 22.8 \times 10^{-6}$ K^{-1}, as well as $\alpha_{Vunit\ cell} = 38.8 \times 10^{-6}$ K^{-1}. These findings provide a precise characterisation and obtain important thermal parameters for the evaluation of its flame retardant properties.

1. Introduction

$ZnCO_3$ has attracted a large amount of attention recently as a useful substance owing to its many fascinating applications in optical, physical, and chemical fields. A natural, stable $ZnCO_3$ crystal, commonly known as smithsonite in mineralogy, is regarded as a valuable gemstone that can appear transparent and also colourful through the various substitution degrees with transition metal ions (e.g. Cu^{2+}, Cd^{2+}, Mn^{2+}, Fe^{2+}) [1–4]. In materials science, ultra-fine ZnO particles have extensive application in electronics, catalysis, medicine, and the chemical industry. Both zinc carbonate hydroxides ($ZnCO_3$ hydroxides) and $ZnCO_3$ are important intermediate substances for the production of ultra-fine ZnO particles [5–7]. The qualities of the ZnO product, including particle size, dispersibility, crystallinity, and purity, closely depend on the properties of carbonate precursors [8,9]. As a frequent occurrence, $ZnCO_3$ hydroxides are sensitive to interact with some adsorbate on surface and thereby cannot ensure high purity to decrease the qualities of decomposition product ZnO. Instead, $ZnCO_3$ can maintain a high chemical stability in the air, where its thermal decomposition process is the simplest; accordingly, it is treated as an optimal precursor for ZnO preparation. In material engineering, $ZnCO_3$, as a high-potential flame retardant material, exhibits multiple integrated advantages in terms of being a flame retardant, a fire extinguisher, and also defending harmful gas

* Corresponding author at: College of Material Science and Engineering, Guizhou Minzu University, Guiyang 550025, China.
** Corresponding author at: State Key Laboratory of Geological Processes and Mineral Resources, China University of Geosciences, Beijing 100083, China.
E-mail addresses: liangwen.pku@163.com (W. Liang), 2014010025@cugb.edu.cn (L. Li).
[1] These authors contributed equally to this work.

https://doi.org/10.1016/j.jallcom.2021.162916
0925-8388/

[10–13]. More concretely, it has excellent flame retardancy and durability that are combined with distinguishing features such as proper decomposition temperature, large thermal absorption, and CO_2 fire extinguishing properties [10,11]. Remarkably, it is effective at absorbing toxic gases that escape from burning organic compounds such as H_2S, SO_2, HCN, etc [12,13]. However, there is no available $ZnCO_3$ analytical reagent at present, and the analogues are dominated by $ZnCO_3$ hydroxides. One reasonable explanation lies in the fact that the strong hydration of Zn^{2+} could impede the acquisition of $ZnCO_3$ from aqueous solutions directly at ambient conditions. For instance, Sharma et al. [14] prepared $ZnCO_3$ using the precipitation reaction of the aqueous solutions of $ZnSO_4$ and Na_2CO_3, yet actually the final product was confirmed as $Zn_5(CO_3)_2(OH)_6$ [14]. Thus, exploring new synthetic routes for the further study and development of $ZnCO_3$ is of great interest in materials science.

To date, a great deal of research has been devoted to optimising synthetic method and some progress has been made. Feng et al. [15] developed the micro-emulsion method to achieve $ZnCO_3$, but the process was too rigorous to be implemented on a large scale [15]. Zhang et al. [16] prepared $ZnCO_3$ successfully via the hydrothermal method from aqueous solutions of $ZnCl_2$ and K_2CO_3 [16]. Wu and Jiang [17] synthesized nanocrystalline $ZnCO_3$ via a solid-state reaction by grounding $ZnSO_4.7\,H_2O$ and NH_4HCO_3 in the presence of a surfactant [17]. Shamsipur et al. [18] also reported the synthesis of $ZnCO_3$ by adding a $Zn(NO_3)_2.7\,H_2O$ solution to a Na_2CO_3 solution on the premise of controlling concentrations, flow rates, and reactor temperatures [18]. In these findings, various techniques were proposed for the successful synthesis of $ZnCO_3$. However, almost all of these products are nanocrystalline, and some obvious limitations still exist in the characterisation of material properties. The nanocrystalline with a lower degree of crystallinity emerges as an amorphous feature that does not ensure a sufficiently high quality for spectrum quantitative analysis, including XRD, Raman, Infrared absorption, etc. For this reason, experimental evaluations of important properties such as crystal structure, lattice vibrations, and constitution water are not entirely clear. Moreover, it is impossible to conduct a composition analysis in such tiny nanoparticles that the purity of as-synthesized $ZnCO_3$ cannot be confirmed. Most importantly, a large amount of adsorbed water and the distinct exothermic crystallisation reaction have a great impact on the measurement of intrinsic thermal properties, thus impeding the accurate characterisation of a flame retardant candidate. To solve such issues as improving progress in $ZnCO_3$ synthetic method, the design of single crystal growth is undoubtedly essential; however, it has not been reported so far.

In this paper, $ZnCO_3$ powder and single crystals were prepared under high P-T while the chemical composition and crystal structure were determined. The thermal stability and the endothermic peak, as well as the heat capacity, were acquired through thermal analysis. As a complement to thermal properties, the accurate thermal expansion of lattice parameters was quantified by single crystal XRD. These results will offer a significant reference for potential applications to explore a new flame retardant.

2. Experimental method

The high P-T experiments were performed on a DS 6 × 600 t cubic-anvil-type apparatus and the assembly consisted of graphite heater and h-BN pressure medium. The sample pellet was designed as the cylinder of 6 mm in diameter and 3 mm in length to reduce temperature and pressure gradient. Two kinds of methods were presented for the $ZnCO_3$ powder preparation. (1) ZnO (99.99%, Alfa Aesar) and anhydrous $H_2C_2O_4$ (98%, Alfa Aesar) were mixed by molar ratio 1: 1.5. The mixture was made into a sample pellet, sealed in a platinum tube (0.1 mm in thickness) and performed at 3 GPa and 973 K for 1 h. (2) $ZnC_2O_4.2\,H_2O$ (99.99%, Alfa Aesar) was made into a sample pellet and covered by platinum foil (0.025 mm in thickness). Then high P-T experiment was carried out at 1 GPa and 773 K for 0.5 h. Subsequently, experiments (1) and (2) were quenched to room temperature before the pressure released. The platinum capsule was cut open and finally $ZnCO_3$ powder sample was obtained. The $ZnCO_3$ single crystals were grew by following high P-T hydrothermal method. The as-synthesized $ZnCO_3$ powder and anhydrous $H_2C_2O_4$ were mixed by molar ratio of 1: 1. The sample pellet was prepared and sealed in a platinum tube together with 30 μL deionized water. It was conducted at 3 GPa and 973 K for 48 h and then quenched to ambient conditions. The platinum tube was opened and the sample was removed, cleaned in deionized water by ultrasonication and finally air-dried.

The single crystals were observed and selected under a plane polarized microscope and the composition was quantified by electron probe microanalysis (EPMA). The elements contents were measured with a JEOL JXA-8230 electron microprobe at Shandong Institute of Geological Sciences, China. Using the as-synthesized crystals, a thin section was polished and plated with lemma of carbon. Energy Dispersive X-Ray Spectroscopy (EDX) was used to identify the type of the elements and also determine the weight percentage (wt%). The operating conditions were 15 kV accelerating voltage, 1 × 10–8 A beam current, and 5 μm beam spot. ZnS was used as standard samples. Matrix effects were corrected using the ZAF software provided by JEOL.

TG and DSC data was determined by a simultaneous thermal analyzer (model: STA 449F3, NETZSCH, Germany). The sample of total 20 mg was heated from 311 K to 937 K with 5 K/min heating rate in the air. The Raman system used for the experiments is a Renishaw 2000 micro-confocal laser Raman spectrometer equipped with a charge-coupled device detector, a 2400 lines mm^{-1} diffraction grating and a holographic notch filter. The spectrum physics model of a 2017 argon ion laser operating at 514.5 nm was used as the excitation source. The laser power was limited to 30 mW to avoid overheating of the sample and the zero-offset was calibrated using a silicon single crystal at 520.0 cm^{-1}. Scattered radiation was collected by an Olympus microscope 20 × at an ultra-length working distance objective through backscattering. The infrared spectrum experiment was performed on a Fourier transform infrared spectrometer (model: VERTEX 7.0, BRUKER).

Single crystal XRD measurements were obtained at ambient conditions with a Rigaku Xtalab PRO diffractometer system and HyPix-6000HE detector. The intensity data were collected using a 1.2 Kw water cooled microfocus source with a Mo rotor target and multilayer mirrors. Data processing was performed with the CrysAlisPro processing program. The structures were determined using direct methods with the SHELXS package and refined in the anisotropic approach for non-hydrogen atoms using the SHELXL program [19]. For the variation temperatures, the selected perfect single crystal has been mounted on a glass fiber. The temperature controlled and measured by a set of OxfordCryosystems, by cooled and heated N_2 gas blowing on to the sample, the sample's temperature can be fixed in the given temperatures. The single crystal date were obtained from cooled or heated sample after 30 mins, to maintain a thermal equilibrium state of the sample. The experiments were carried out from 150 K to 383 K for the variable temperatures.

3. Results and discussion

3.1. The powder synthesis and single crystals growth of $ZnCO_3$

Despite the common occurrence of ore-forming smithsonite in nature, Zn-bearing carbonates generally tend to form $ZnCO_3$ hydroxides due to the sensitive hydrolysis of Zn^{2+}. For this reason, the issue of inhibiting the Zn^{2+} hydrolysis reaction while ensuring the thermal stability of carbonate phase is the key to $ZnCO_3$ synthesis. From the previous studies, the hydrolysis reaction of Mg^{2+} in magnesium carbonates can be inhibited by the high P-T effectively, which can more precisely be attributed to the extreme stability of anhydrous $MgCO_3$ at an ultra-high pressure [20,21]. Likewise, $ZnCO_3$ still maintains structural stability and no phase transition occurs until the pressure reaches 50 GPa [22]. In this case, the anhydrous $ZnCO_3$ phase could be treated as a high P-T quenchable phase that would be more stable than all hydroxide analogues under high pressure extreme conditions, whereas its poor thermal stability could be significantly enhanced. It is thus conceivable that the powder synthesis and crystal growth are expected to be feasible under high P-T conditions.

To date, there have not been any studies on the thermal stability of $ZnCO_3$ at high pressure. Nevertheless, its thermal stability could be close to $FeCO_3$ according to striking structural similarities [23], and the trial experiment conditions were fixed to 3 GPa and 973 K. High P-T annealing reaction (2) was designed in a fully-closed cavity, while the sufficient CO_2 atmosphere was provided by the decomposition reaction (1).

$$H_2C_2O_4 \rightarrow CO_2 + CO + H_2O \quad (1)$$

$$ZnO + CO_2 \rightarrow ZnCO_3 \quad (2)$$

As shown in Fig. 1(a), the powder XRD pattern of the as-synthesized sample and all diffraction peaks can be indexed as the $R\bar{3}c$ calcite-type structure. The XRD pattern shows a high quality with a strong intensity, sharp diffraction peaks, and smoothed baseline, all of which indicate that $ZnCO_3$ powder was pure with a high degree of crystallinity. Here, the powder XRD data were used for phase identification and the accurate lattice parameters were given by single crystal XRD data in the text below.

Compared with the previous reports of $ZnCO_3$ synthesis, the principle of high P-T reaction (2) is the simplest, that is, high pressure inhibiting the hydrolysis of Zn^{2+}. Besides this, high P-T conditions can not only enhance the diffusive rate but also decrease activation energy of reactions, such that $ZnCO_3$ can be achieved within 1 h through accelerating the reaction rate substantially. Further more, $ZnCO_3$ with various doping concentrations (eg: Fe^{2+}, Mn^{2+}, Cu^{2+}) can be prepared by reaction (2) using the mixture of corresponding oxides (ZnO, Fe_2O_3, MnO_2, CuO), whereas the CO reduced atmosphere can ensure the stability of divalent ions. In this way, the more quantitative study for $ZnCO_3$ with complex chemical compositions could be carried out.

To further extend the understanding of high P-T reactions, the high P-T decomposition of $ZnC_2O_4.2\,H_2O$ is proposed to synthesize $ZnCO_3$. At ambient pressure, the thermal decomposition of $ZnC_2O_4.2\,H_2O$ is described as.

$$ZnC_2O_4.2\,H_2O \rightarrow ZnO + CO_2 + CO + 2\,H_2O \quad (3)$$

In contrast to this, the decomposition temperature of $ZnC_2O_4.2\,H_2O$ and $ZnCO_3$ could be completely separated in the P-T diagram because the both have the significant differences in high P-T stability. The thermal decomposition of $ZnC_2O_4.2\,H_2O$ induced by the pressure can be divided into two steps:

$$ZnC_2O_4.2\,H_2O \rightarrow ZnCO_3 + CO + 2\,H_2O$$

$$ZnCO_3 \rightarrow ZnO + CO_2 \quad (4)$$

During this process, $ZnCO_3$ phase acts as a "hidden phase" in the P-T diagram, presented as the higher the pressure, the wider the phase region. The detail description of the phase separation was attached in Supplementary Figure 1. Specifically, some appropriate high P-T conditions could maintain $ZnCO_3$ stability while undergoing $ZnC_2O_4.2\,H_2O$ decomposition, and it is expected to prepare $ZnCO_3$. A half-open cavity was created by the platinum foil to ensure a rapid reaction by actively releasing the decomposition CO and H_2O. Fig. 1(b) gives the powder XRD pattern of the product from the decomposition of $ZnC_2O_4.2\,H_2O$ at 1 GPa and 737 K for 0.5 h, and the data quality is comparable to what was obtained from the high P-T annealing reaction.

Compared with the fully-closed cavity in the reaction (2), the half-open assembly of the reaction (4) are much simpler; that is, only appropriate high P-T conditions are required. Therefore, this method and principle may have the application prospect of large-scale production of $ZnCO_3$. Now that the phase stability region of

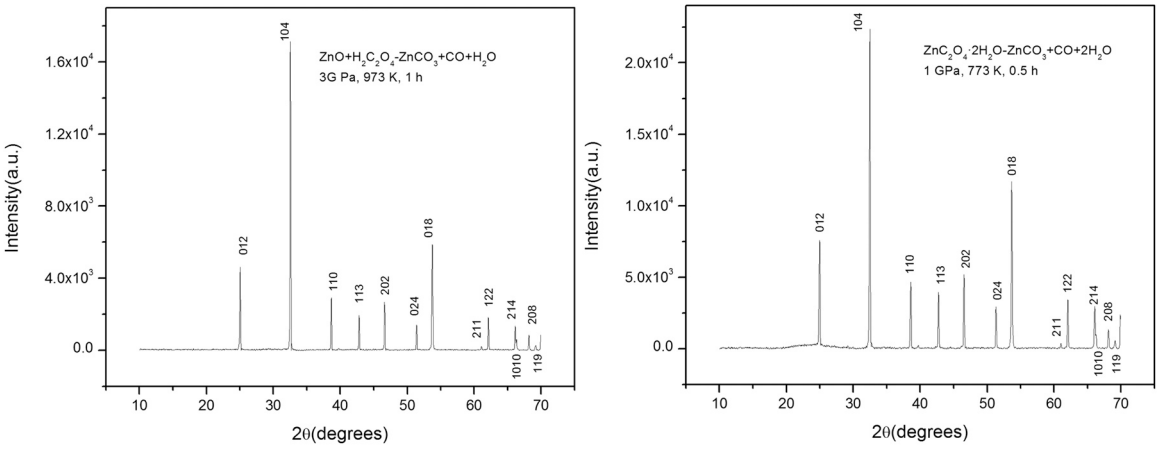

Fig. 1. The powder XRD patterns of $ZnCO_3$ synthesized under high P-T from the different ways: (a) $ZnO + H_2C_2O_4 \rightarrow ZnCO_3 + CO + H_2O$ (3 GPa, 973 K, 1 h); (b) $ZnC_2O_4.2\,H_2O \rightarrow ZnCO_3 + CO + 2\,H_2O$ (1 GPa, 773 K, 0.5 h).

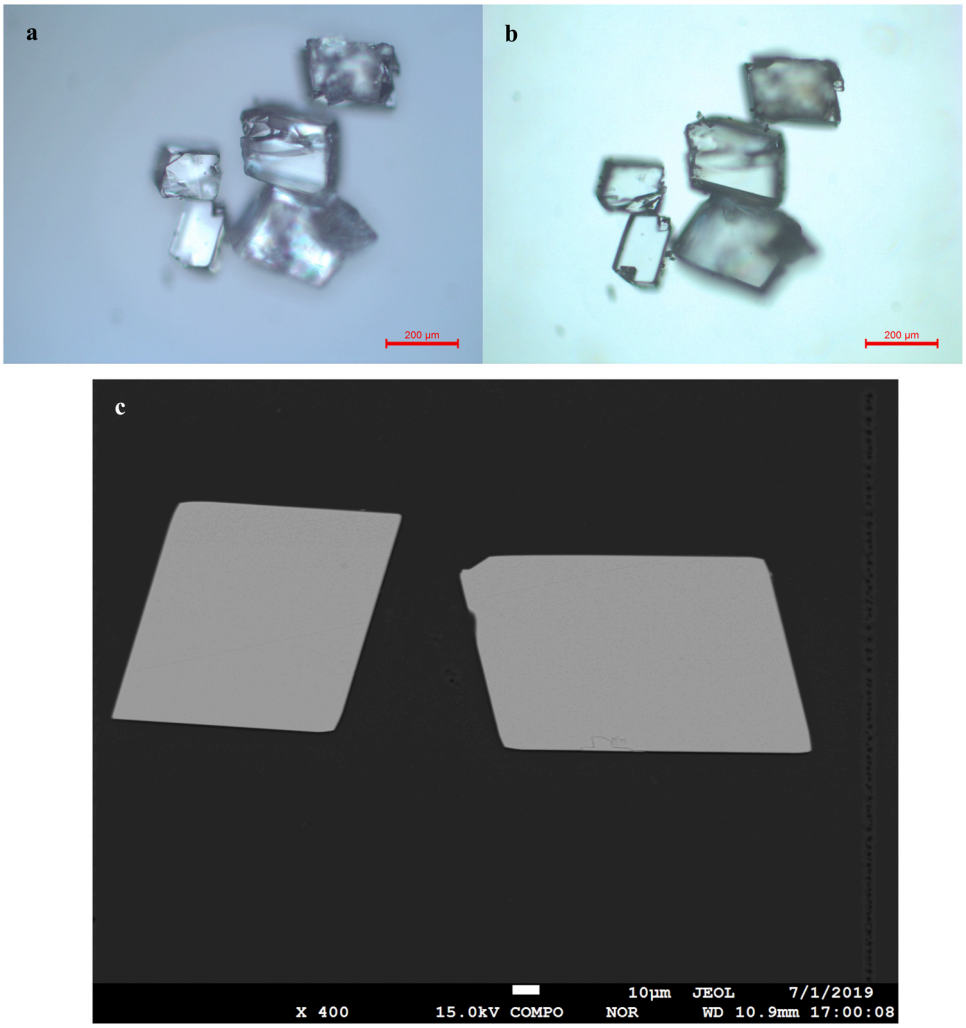

Fig. 2. The micrograph for $ZnCO_3$ single crystals observed in a polarizing microscope with reflected light (a) and transmitted light (b), and the BSE image (c) of $ZnCO_3$ single crystals thin section.

$ZnC_2O_4.2\,H_2O$ and $ZnCO_3$ can be separated in the P-T diagram, a limit low pressure is proposed to exist for the preparation of $ZnCO_3$. In this case, an extended question remains; namely, whether this limit low pressure is within the range of industrial ammonia production (30–50 MPa). If true, the large-scale production of $ZnCO_3$ could be realized using available industrial technologies. The decomposition reaction (4) is thus worth further investigation under low P-T regions.

Using as-synthesized $ZnCO_3$ powder as the starting material, $ZnCO_3$ crystals were cultivated during process of the dissolution-crystallisation in the high P-T saturated solution. The equilibrium can be described as (5), in which the hydrolysis of Zn^{2+} was completely inhibited by high pressure conditions.

$$ZnCO_3 \leftrightarrow Zn^{2+}_{(aq)} + CO_{3(aq)}^{2-} \leftrightarrow ZnCO_3 \quad (5)$$

(powder) (saturated solution) (crystals)

The CO_2 +H_2O environment acts as the acidic medium for the aqueous solution to not only promote $ZnCO_3$ powder dissolution but also further prevent the formation of OH^-. In addition, the H_2O fluid plays an important role in reducing the residual stress in single crystals.

Table 1
Elements contents quantified by EDX.

Elements	Weight percentage	Atomic percentage
C K	7.85	16.88
O K	38.30	61.84
Zn L	53.85	21.28
Total	100.00	

3.2. Morphology and composition of $ZnCO_3$ single crystals

From the microscope observations, the as-synthesized $ZnCO_3$ crystals exhibited perfect rhomboid morphology up to 200 μm in sizes; the 120° edge angle is a typical (101) cleaving behaviour of calcite-type materials, as shown in Fig. 2(a)(b). The crystals appeared colourless and transparent, whereas the dark inclusions on the surface were $ZnCO_3$ fine powder as the precipitation from the saturated solution.

The chemical composition is an important criterion in the assessment of crystal qualities. According to the EDX results, the crystals contain C, O and Zn, and other elements were not detected,

Table 2
The crystal structure of $ZnCO_3$.

Space group $R\bar{3}c$ ***Lattice parameters.***											
		a Å	c Å	α°	β°	γ°	V Å³	Zn-O Å	O Å	Zn-O°	R
$ZnCO_3$	Synthetic sample	4.6463(3)	15.0015(11)	90	90	120	280.47(4)	2.1070(7)	1.2851(15)	88.41(3)	0.0229
	Natural smithonite	4.6526(7)	15.0257(22)	90	90	120	281.68(13)	2.1107(6)	1.2859(6)	–	0.013
Natural smithonite is $Zn_{0.975}Mg_{0.006}Fe_{0.015}Mn_{0.003}CO_3$[24].											
Positional and thermal parameters											
$ZnCO_3$											
Parameters	Zn	C	O								
x	0	0	0.2766(3)	0.27636(11)*							
y	0	0	0								
z	0	1/4	1/4								
U11	0.0057(5)	0.012(3)	0.0054(7)								
U22	0.0057(5)	0.012(3)	0.0071(7)								
U33	0.0081(6)	0.002(4)	0.0085(9)								
U23	0.000	0.000	-0.0014(3)								
U13	0.000	0.000	-0.00072(17)								
U12	0.0029(2)	0.0059(14)	0.0035(3)								

* is the atomic positions of natural smithonite Zn0.975Mg0.006Fe0.015Mn0.003CO3 given by Effenberger et al. [24].

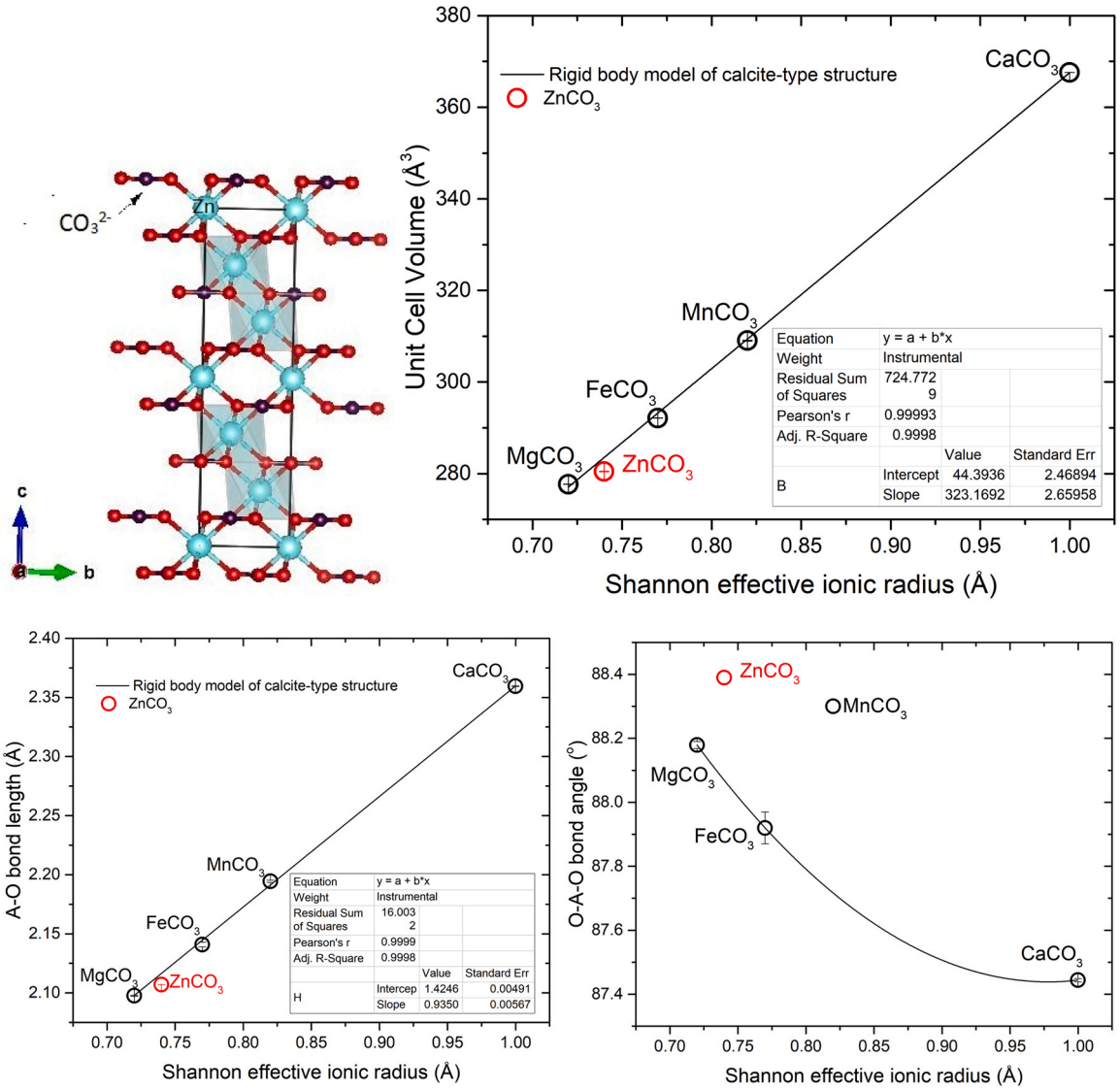

Fig. 3. Crystal structure of $ZnCO_3$, plotted into the calcite-type rigid body model, in which the crystal structures were referenced from $MgCO_3$ [26], $FeCO_3$ [27], $MnCO_3$ [28], and $CaCO_3$ [29].

seen Supplementary Figure 2. Fig. 2(c) and Table 1 shows the backscattering electron (BSE) and elements contents quantified by EDX. The Zn wt% of 53.85% is approaching to the theoretical value 52.14% calculated by the ideal formula for $ZnCO_3$. The grayscales of the polished crystals surfaces were almost identical from the BSE images, thus indicating that the composition of the crystals was homogeneous.

3.3. Crystal structure of $ZnCO_3$

The accurate structural data of the as-synthesized $ZnCO_3$ crystals were quantified using single crystal XRD, corresponding to the lattice parameters, positional and thermal parameters, and bond length and angle, and are summarized in Table 2, together with the natural smithsonite ($Zn_{0.975}Mg_{0.006}Fe_{0.015}Mn_{0.003}CO_3$) for comparison [24]. The result was formatted into a CIF file, which is attached as Supplementary materials. As shown in Fig. 3, $ZnCO_3$ has a$R\bar{3}c$rhombohedral structure with common calcite-type features [25]. Specifically, the carbonate ions (CO_3^{2-}) are restrained by strong internal C-O bonds and interlinked with the cations Zn^{2+} by weaker Zn-O bonds. The Zn atom is located in the center of the (ZnO_6) octahedron as the Zn atom is located at position 6(b) (0, 0, 0) with site symmetry$\bar{3}$; C atom at position 6(a) (0, 0, 1/4); O atom at position 18(e) (x, 0, 1/4), which is consistent with the previous results given by Effenberger et al. [24]. A slight deviation in x value of O atomic position and differences in lattice parameters are caused by the Mg^{2+}, Fe^{2+}, and Mn^{2+} impurities in natural smithsonite. The central ion Zn^{2+} has six-coordinates and is in a slightly tilting (ZnO_6) octahedron by equal Zn-O bond lengths. The Zn-O bond length (2.1070(7) Å) that we obtained is in good agreement with those in other Zn^{2+}-bearing carboxylate complexes [28]. The O-Zn-O angle, as a deviation (88.41(3)) from the regular octahedron (90°), is caused by a hybridisation between the Zn^{2+} and O^{2-} valence electronic orbitals. Overall, the (ZnO_6) octahedron tends more toward the regular octahedron than those of other calcite-type structures ($CaCO_3$, $MgCO_3$, $FeCO_3$, and $MnCO_3$) [26–29].

Effenberger et al. [24] modelled calcite-type structural parameters using natural minerals close to the end-member compositions as a basic reference for the field of crystal chemistry [24]. Most recently, Liang et al. [28] further optimised the calcite-type ACO_3 model using synthetic single crystals with a view to avoiding the influence of impurities [28]. By using the Shannon effective ionic radius to quantify the cation substitution [30], the behaviour of a unit cell volume ($V_{\text{unit cell}}$) and A-O bond length (*A-O*) for four end members ($MgCO_3$, $FeCO_3$, $MnCO_3$, and $CaCO_3$) obeys a linear relationship with a good correlation R^2, described in (6) and (7):

$$V_{\text{unit cell}} = 44{\cdot}394 + 323{\cdot}1692 \times r \ (R^2 = 0.9998) \quad (6)$$

$$A\text{-}O = 1{\cdot}4246{+}0{\cdot}9350 \times r \ (R^2 = 0.99989) \quad (7)$$

This perfect linear relationship between $V_{\text{unit cell}}$ and *A-O* is strong evidence that the rigid body model is valid for simulating the substitution of various cations in the calcite-type lattice.

Based on this, the $ZnCO_3$ crystal structure was plotted into the calcite-type rigid model for a better understanding, as seen in Fig. 3. However, the experimental $V_{\text{unit cell}}$ and *A-O* (280.47(4) Å^3 and 2.1070(7) Å) are evidently lower than the calcite-type rigid model. There are a few potential explanations for abnormal behavior of $ZnCO_3$. As a criterion in crystal chemistry, the Shannon ionic radius describes the substitution in ionic bonds more effectively, rather than covalent bonds. Zn^{2+} has much larger electronegativity (1.66) than Mg^{2+} (1.23) such that the Zn-O bond tends to a covalent bond. In spite of both having nearly equal radii, the hybridisation between the Zn^{2+} and O^{2-}(S^{2-}) could form a short Zn-O(S) bond due to the binding of valence electrons, which prefers four coordinates (e.g. zincite ZnO, sphalerite ZnS); in contrast to this, the Mg-O bond is a typical ionic bond so that Mg^{2+} tends to form six coordinates (e.g. periclase MgO, magnesium silicate Mg_2SiO_4). For this reason, $ZnCO_3$ is deemed as a minority case as Zn^{2+} has six coordinates, which leads to a slight mismatch when using the Shannon ionic radius Zn^{2+} (0.745 Å) to measure the Zn-O covalent bond. Here, we believe that the calcite-type rigid model would be indisputable and then revise the effective radius of Zn^{2+} in the $ZnCO_3$ structure. We substituted the experimental data ($V_{\text{unit cell}}$=280.47(4) Å^3 and *A-O* = 2.1070(7) Å) into the formula (6)(7) and calculated the Zn^{2+} radius to be 0.73 Å, which could serve as a reference for similar compounds with Zn^{2+} six-coordination.

3.4. Raman and infrared spectrum

The Raman vibrations of $ZnCO_3$ offer complementary information on the crystal structure, and were achieved from the as-synthesized single crystals. In Fig. 4(a), six Raman active vibrations within a wavelength of 100–2000 cm^{-1} were easily distinguished by the sharp peaks located at 190.24(5), 298.90(3), 735.50(7), 1091.18(4), 1404.37(2), and 1729.44(7) cm^{-1}, which becomes the standard of Raman spectrum of $ZnCO_3$. The peaks at 190.24(5) cm^{-1} and 298.90(3) cm^{-1} are identified as a translational lattice mode *T* and a librational lattice mode *L*, respectively. The peaks at 735.50(7) cm^{-1} come from an in-plane bending internal mode ν_4. The peaks with the strongest intensity located at 1091.18(4) cm^{-1} are a result of the symmetric stretching of the internal mode ν_1. Similarly, the peaks at 1404.37(2) cm^{-1} and 1729.44(7) cm^{-1} are caused by the antisymmetric stretching mode ν_3 and an out-of-plane bend $2\nu_2$, respectively.

Since the $ZnCO_3$ crystals were obtained in a high water fugacity environment, the characterization of the infrared absorption spectrum is necessary to verify the anhydrous performance. The infrared absorption was measured within a range of 400–4000 cm^{-1}, as shown in Fig. 4(b), in which three infrared active bands were observed at 876 cm^{-1}, 1408 cm^{-1}, and 1507 cm^{-1}. Using a reference to the present literature on $MgCO_3$ [31,32], these are, respectively, assigned to the internal vibrational modes of the CO_3^{2-} ions in the$R\bar{3}c$structure as the out-of-plane bending ν_2 (A_2), TO component of ν_3 (E_u) asymmetric stretching, and the LO component of ν_3 (E_u). Importantly, no remarkable peak was distinguished within the range of 3000–4000 cm^{-1}, indicating that the $ZnCO_3$ crystals do not contain constitution water (OH^-) and surface-adsorbed water. It has therefore been proven to be an anhydrous phase.

3.5. TG and DSC analysis of $ZnCO_3$ single crystals

TG and DSC analysis, as a basic approach to studying the thermal decomposition process, has been used widely in materials science. In fact, accurate thermal analysis data are essential for the evaluation of $ZnCO_3$ that could assist in identifying a candidate for flame retardants. However, the previous results make it difficult to perform a quantitative analysis owing to the poor data quality obtained from $ZnCO_3$ nanocrystalline [17]. The adverse effects could be caused by the following factors:

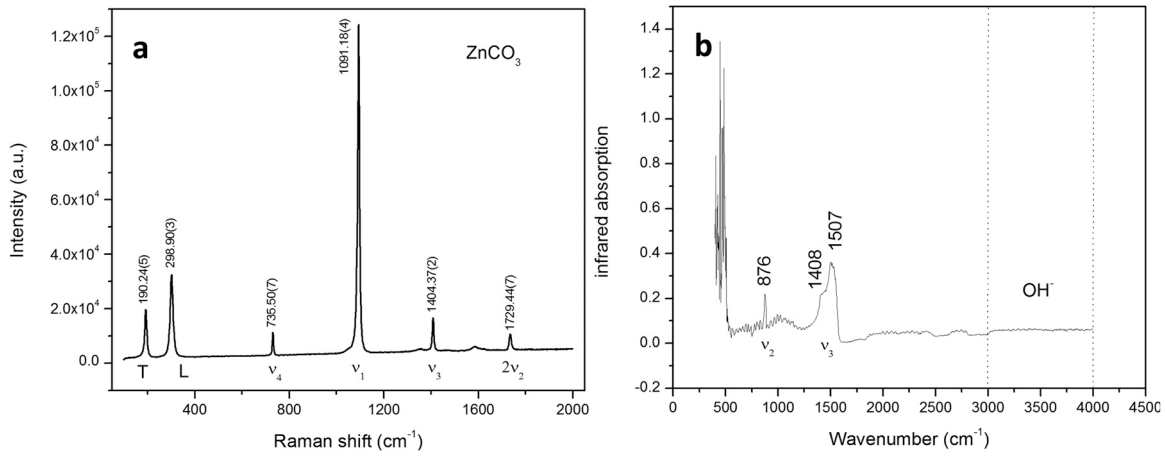

Fig. 4. Raman spectrum (a) and infrared absorption (b) of $ZnCO_3$ single crystals.

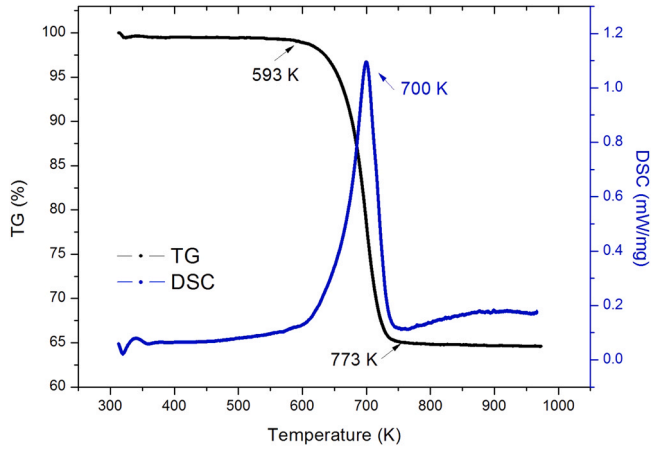

Fig. 5. The TG and DSC analysis of $ZnCO_3$ single crystals.

(1) Caused by a large amount of surface-adsorbed water, the nanocrystalline appeared to lose weight before 373 K, thus causing an obvious deviation between the experimental and theoretical values of TG;
(2) During the heating process, the hydrolysis reaction may occur in the coexistence of $ZnCO_3$ and H_2O to form $ZnCO_3$ hydroxides, and, correspondingly, the additional formation of hydroxides can greatly interfere with the original DSC curve of anhydrous $ZnCO_3$;
(3) An exothermic crystallisation reaction cannot be neglected when heating nanocrystalline. Thus, the behaviour of a measured DSC curve was attained with obvious irregularity and was overlapped by an exothermic background. Accordingly, it is impossible to quantify the accurate thermal parameters (e.g. heat capacity and endothermic peak) from the relevant DSC data.

Conversely, the thermal analysis data on $ZnCO_3$ single crystals are expected to be beneficial in overcoming these adverse effects; in particular, by not only avoiding a crystallisation reaction but also ruling out constitution water and surface-adsorbed water. The TG and DSC profiles of $ZnCO_3$ single crystals heated from 311 K to 973 K are presented in Fig. 5. The TG value at 593 K was 99.2% attributed to tiny amounts of adsorption water (< 1%) on the surface of the crystals. Subsequently, TG began to lose weight, particularly above 593 K,

Table 3
Flame retardant properties of $ZnCO_3$.

Flame retardant	Initial decomposition temperature	Final decomposition temperature	Endothermic peak	Ref.
$ZnCO_3$	593 K	773 K	109.64 kJ/mol 0.874 kJ/g	This work
$MgCO_3$	693 K	873 K	128.59 kJ/mol 1.531 kJ/g	[21]
$Mg(OH)_2$	603 K	673 K	80.07 kJ/mol 1.373 kJ/g	[35]
$Al(OH)_3$	503 K	673 K	91.40 kJ/mol 1.172 kJ/g	[35]

while the decomposition reaction occurred. The rate of decomposition became remarkable between 673 K and 723 K, accompanied by one sharp endothermic peak in the DSC curve. The TG did not show any obvious change above 737 K, which is evidence that the $ZnCO_3$ crystals had been entirely decomposed into ZnO. The final TG value maintained a constant of 63.8%, which is consistent with the theoretical value of 64.9% within the margin for error. Significantly, before the decomposition, the DSC curve exhibited a smooth upward trend without any perturbation from exothermic peaks, revealing that the crystals underwent a continuous endothermic process and had no exothermic crystallisation. On this basis, we fitted the DSC curve from 373 K to 573 K, and the quantity of heat (Q) and the heat capacity (C_p) as a function of temperature (T) can be calculated using Maier-Kelley equation [33]:

$$Q(T) = -0.31637T + 0.00253T^2/2 - 2037.8706/T \quad (8)$$

$$C_p(t) = -39.679 + 0.317T + 255589.731/T^2 \quad (9)$$

where T is the kelvin units of temperature ranged from 373 K to 573 K, and the unit of C_p is J/(mol·K), and the unit of Q is J/g. The details can be seen in the Supplementary materials. The C_p could be thought to be an important thermal parameter for describing the endothermic behaviour before decomposition. Furthermore, the decomposition temperature was confirmed to be between 593 K and 773 K, while the endothermic peak (ΔQ) can be quantified by (10) according to the DSC curve:

$$\Delta Q = \int_{593K}^{773K} DSC(t)dt = 874.16\text{J/g} = 109.64\text{kJ/mol} \quad (10)$$

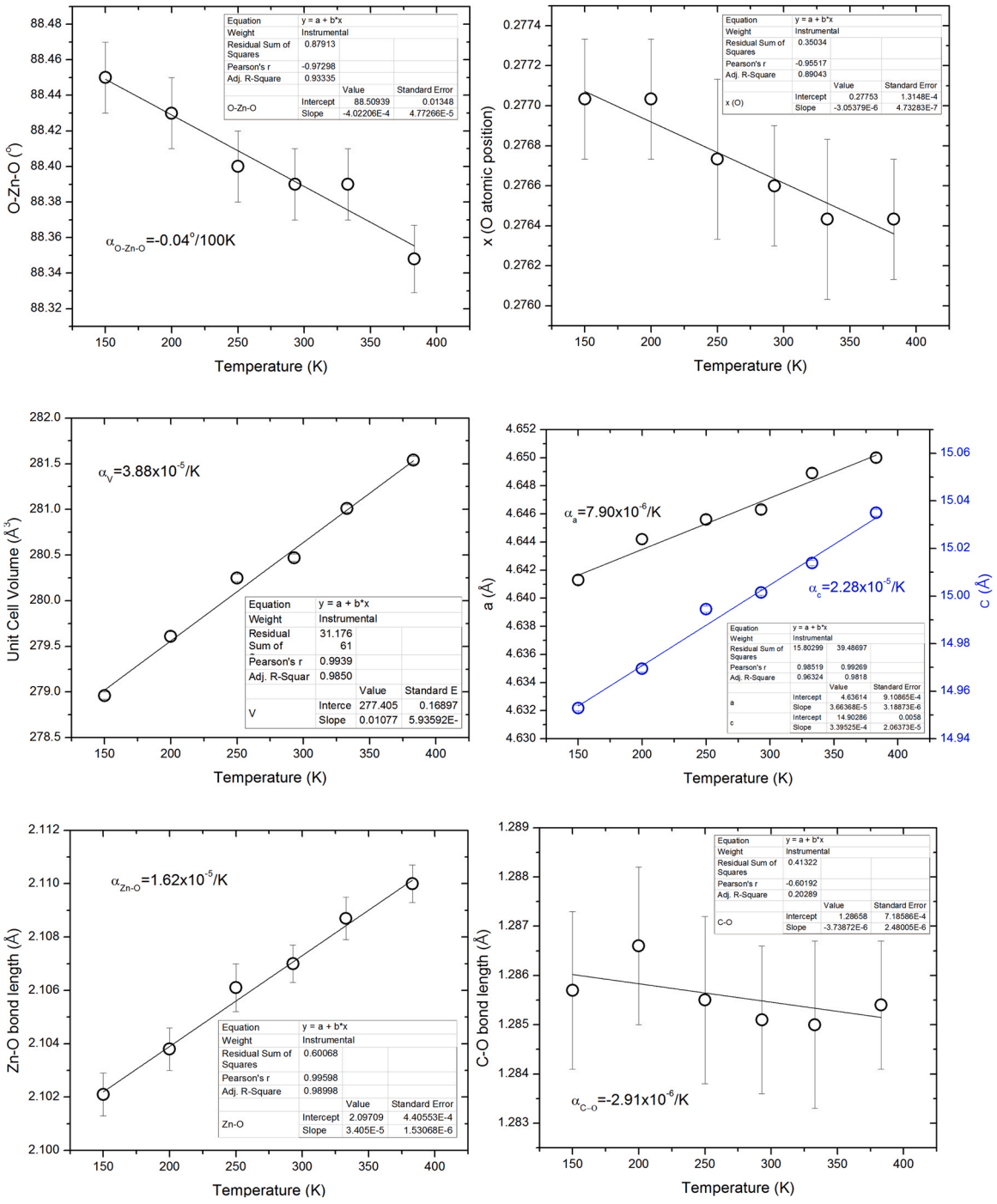

Fig. 6. The thermal expansion of $ZnCO_3$ single crystal.

The decomposition temperature and the endothermic peak are the main indices for measuring the performance of flame retardants. The thermal properties of common flame retardants are summarised in Table 3 for comparison with $ZnCO_3$ [34–36]. Obviously, the decomposition temperature of $ZnCO_3$ is halfway between $MgCO_3$ and hydroxides ($Mg(OH)_2$ and $Al(OH)_3$), which can cover the ignition point of common substances to satisfy the fire safety regulatory standards. The decomposition heat per unit molar is close to that of $MgCO_3$ and is higher than hydroxides; conversely, its decomposition heat by a unit mass is the lowest due to the large molar mass of $ZnCO_3$. In accordance with the comparison data, even though the flame retardancy of $ZnCO_3$ is not as good as $MgCO_3$, the CO_2 fire extinguishing and chemical stability of the two carbonates are far superior to hydroxides. Except for fire resistance, $ZnCO_3$ is able to react rapidly with toxic gases from burning organic compounds to form stable compounds; in this regard, $MgCO_3$ cannot be trusted to

Table 4
(a). Single crystal XRD of $ZnCO_3$ at different temperatures.

Temperature	150 K	200 K	250 K	293 K	333 K	383 K	
a	4.6413(3)	4.6442(4)	4.6456(3)	4.6463(3)	4.6489(3)	4.6500(3)	
c	14.9529(12)	14.9694(14)	14.9945(13)	15.0015(11)	15.0139(11)	15.0350(14)	
$V_{unit\ cell}$	278.96(4)	279.61(5)	280.25(4)	280.47(4)	281.01(4)	281.54(4)	
Zn-O	2.1021(8)	2.1038(8)	2.1061(9)	2.1070(7)	2.1087(8)	2.1100(7)	
C-O	1.2857(16)	1.2866(16)	1.2855(17)	1.2851(15)	1.2850(17)	1.2854(13)	
O-Zn-O	88.45(2)	88.43(2)	88.40(2)	88.39(2)	88.39(2)	88.348(19)	
x (O position)	0.2770(3)	0.2770(3)	0.2767(4)	0.2766(3)	0.2764(4)	0.2764(3)	
(b). Thermal expansion coefficient ($\times 10^{-6}$ K^{-1} or $^oC^{-1}$) of calcite-type ACO_3 carbonates at ambient pressure							
ACO_3	A-O /K(°C)	O-A-O**°/100 K(°C)**	C-O /K(°C)	**V** /K(°C)	**a** /K(°C)	**c** /K(°C)	Anisotropy α_c/α_a
$ZnCO_3$ This study	16.2	-0.04	-2.91	38.8	7.90	22.8	2.89
$MnCO_3$[26]	12.14	-0.05	-3.67	28.49	5.08	18.06	3.56
$MgCO_3$*[34]	15.8	-0.07	-4.6	36.4	6.75	22.9	3.39
$CaCO_3$*[34]	15.9	-0.1	-22.6	26.7	-2.8	32.3	–

$MgCO_3$* is natural magnesite: $Mg_{0.998}Ca_{0.002}CO_3$ and **$CaCO_3$*** is natural calcite: $Ca_{0.998}Mg_{0.002}CO_3$. [29]

perform. Hence, $ZnCO_3$ is an excellent flame retardant as well as $MgCO_3$, and both of the candidates will be developed and utilised in the future to replace traditional flame retardants.

3.6. The thermal expansion of $ZnCO_3$ single crystals

To further evaluate a flame retardant material, the thermal expansion property is an essential parameter for judging the plasticity and affinity of ceramic materials. For this reason, we used as-synthesized $ZnCO_3$ crystals to investigate accurate thermal expansion using single crystal XRD including lattice parameters and (ZnO_6) octahedron geometry. Fig. 6 and Table 4(a)(b), together with other calcite-type carbonates [28,29], give the variations in lattice parameters (*a* and *c*), unit cell volume ($V_{unit\ cell}$), bond length (*Zn-O* and *C-O*), and bond angle (*O-Zn-O*) as functions of temperature (*T*), which can be linearly modelled as (11):

$$\begin{aligned}
&a = 4.63614 + 3.6637 \times 10^{-5}T\,(\alpha_a = 7.90 \times 10^{-6}K^{-1}),\\
&c = 14.90286 + 3.3953 \times 10^{-4}T\,(\alpha_c = 22.8 \times 10^{-6}K^{-1}),\\
&V_{\text{unit cell}} = 277.405 + 1.077 \times 10^{-2}T\,(\alpha_{V\ \text{unit cell}} = 38.8 \times 10^{-6}K^{-1}),\\
&(Zn-O)_{\text{bond length}} = 2.0971 + 3.405 \times 10^{-5}T\,(\alpha_{Zn-O} = 16.2 \times 10^{-6}K^{-1}),\\
&(C-O)_{\text{bondlength}} = 1.2866 - 3.7387 \times 10^{-6}T\,(\alpha_{C-O} = -2.91 \times 10^{-6}K^{-1}),\\
&(O-Zn-O)_{\text{bondangle}} = 88.51 - 4.022 \times 10^{-4}T\,(\alpha_{O-Zn-O} = -0.04^o/100K).
\end{aligned} \tag{11}$$

An approximate relationship of $\alpha_{V\text{unit cell}} \approx 2\alpha_a + \alpha_c$ is verified for the rhombohedral structure, whereas the axial thermal expansivity presents substantial anisotropy (α_c/α_a=2.89). The values of α_a, α_c, and $\alpha_{V\text{unit cell}}$ (7.90×10^{-6} K^{-1}, 22.8×10^{-6} K^{-1}, and 38.8×10^{-6} K^{-1}) are somewhat close to the value of $MgCO_3$ (6.75×10^{-6} $^oC^{-1}$, 22.9×10^{-6} $^oC^{-1}$, and 36.4×10^{-6} $^oC^{-1}$), although there are obvious differences with $CaCO_3$ and $MnCO_3$. This means that the thermal expansivity of calcite-type ACO_3 varies with an A^{2+} ionic radius as it is closely dependent on the A-O bond length. Specifically, the Zn-O bond length (2.1070(7) Å) has a nearly equal thermal expansion coefficient ($\alpha_{A\text{-}O}$ = 16.2×10^{-6} K^{-1}) with regard to the Mg-O bond length (2.0976(4) Å) in $MgCO_3$ ($\alpha_{A\text{-}O}$ = 15.8×10^{-6} $^oC^{-1}$), but is much larger than that of $MnCO_3$ ($\alpha_{A\text{-}O}$ = 12.14×10^{-6} $^oC^{-1}$) owing to the long Mn-O bond length (2.1945(9) Å), which is consistent with general thermal expansion mechanisms. Unlike these, almost all of the thermal expansion coefficients of $CaCO_3$ demonstrate abnormal features that originate from the remarkable thermal shrinkage of the C-O bond length ($\alpha_{C\text{-}O}$ =-22.6×10^{-6} $^oC^{-1}$), even causing a negative thermal expansion along the *a*-axis (α_a =-2.8×10^{-6} $^oC^{-1}$). As a comparison, the C-O bond length in $ZnCO_3$ displays a smaller thermal shrinkage ($\alpha_{C\text{-}O}$ = -2.91×10^{-6} K^{-1}) than those of others such that the thermal expansivity along the *a*-axis is the largest. The reason for this is the fact that the thermal shrinkage of CO_3^{2-} plays an important role in controlling the thermal expansion in the *a-b* plane because the orientation of the CO_3^{2-} ion is parallel to (001). Similar to the behaviour of other ACO_3 [37], the bond angle (*O-Zn-O*) decreases at a rate of 0.04°/100 K, indicating that the thermal expansion and tilting of (ZnO_6) octahedron simultaneously occurs when the temperature increases. As well as these, the O 18(e) atomic position (x, 0, 1/4) moves slightly, and the correspondence as a function of temperature (*T*) can be fitted as (12):

$$x(\text{oxygen atomic position}) = 0.27753 - 3.05379 \times 10^{-6}T \tag{12}$$

As a linear extrapolation, this formula could be used to estimate $ZnCO_3$ structural data at higher temperatures until its decomposition.

3.7. The ZnO product from the thermal decomposition and recrystallisation

As mentioned above, $ZnCO_3$ is deemed to be the optimal precursor in the preparation of ultrafine ZnO particles. However, the as-decomposed ZnO particles could increase in size at a high temperature because the exothermic crystallisation of the final product was distinguished by the nonmonotonic behaviour of DSC ranging from 773 K to 973 K. To understand the recrystallisation process in detail, the variation between the sizes of ZnO particles and the heating time was observed when the decomposition condition of $ZnCO_3$ was fixed at 773 K. In Fig. 7(a)(b)(c), the SEM images showed the morphology of ZnO particles. After 2 h heating, ZnO exhibited ultrafine particles, which has essentially been identified as an amorphous feature. It dispersed as a loose and cotton-shaped morphology due to the release of CO_2. An annealing time of 6 h produced some tinny ZnO crystals (~1 μm) through recrystallisation. By increasing the heating time to 24 h, the ZnO crystals increased in size to 10–50 μm, whereas the morphology exhibited rhombus overall. In accordance with the results of our experiments, using the thermal decomposition of $ZnCO_3$ at a rapid heating time is effective in the preparation of ultrafine ZnO particles.

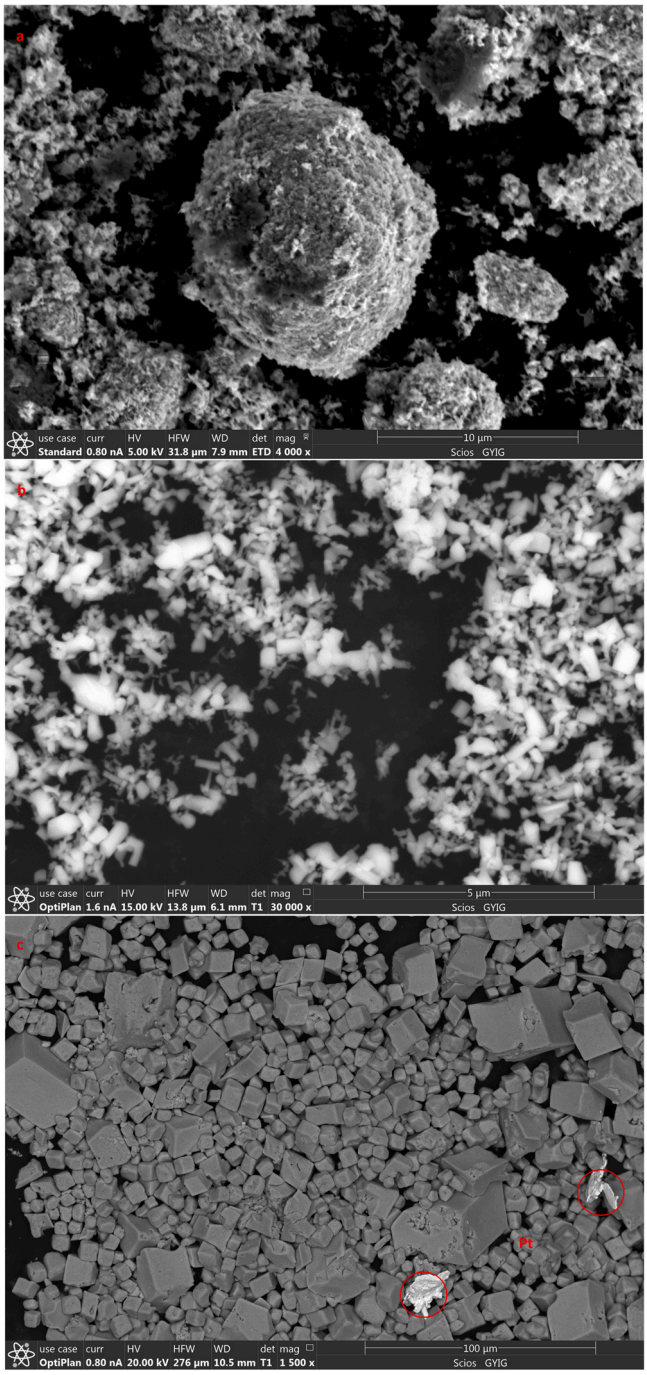

Fig. 7. The ZnO product from the thermal decomposition of $ZnCO_3$ crystals at 773 K, by heating time for 2 h (a), 6 h (b), and 24 h (c). (The white flakes marked by the red circle were identified as the residue coming from platinum capsule).

4. Conclusions

Considering the limitations of the previous synthesis of $ZnCO_3$, we proved that the high P-T synthesis is feasible, and the principle is simple and easy to realize. The crystal structure, the spectral data and the thermal properties were determined, and these results will serve as a pioneer in the research of $ZnCO_3$ flame retardants. On this basis, the thermal and chemical stability of $ZnCO_3$ is worth further investigation under low P-T regions, which could contribute to the development of industrial conditions for large-scale production. An ambitious program for $ZnCO_3$ flame retardant, particularly in combination with the process of inorganic carbon sequestration, may be launched to promote the application in the future.

CRediT authorship contribution statement

Wen Liang: Investigation, Conceptualization, Methodology, Writing – original draft, Writing – review & editing. **Jie Bai:** Investigation, Methodology, Writing – original draft. **Zengsheng Li:** Methodology, Investigation. **Yong Meng:** Methodology, Investigation. **Kaixiang Liu:** Methodology, Investigation. **Lin Li:** Investigation, Conceptualization, Methodology, Writing – original draft, Writing – review & editing.

Declaration of Competing Interest

The authors declare that they have no known competing financial interests or personal relationships that could have appeared to influence the work reported in this paper.

Acknowledgments

We appreciate two anonymous reviewers for their valuable comments and suggestions, which are important to greatly improve the manuscript quality. This study was financially supported by the National Science Foundation for Young Scientists of China (41802044), National Natural Fund of China (4160030283) and the Western Light China (Y8CR028).

Appendix A. Supporting information

Supplementary data associated with this article can be found in the online version at doi:10.1016/j.jallcom.2021.162916.

References

[1] M. Hitzman, N. Reynolds, D. Sangster, C. Allen, C. Carman, Classification, genesis and exploration guides for nonsulfide zinc deposits, Econ. Geol. 98 (2003) 685–714.
[2] M. Böettcher, The formation of rhodochrosite-smithsonite ($MnCO_3$-$ZnCO_3$) solid-solutions at 5o C, Mineral. Mag. 59 (1995) 481–488.
[3] M. Samouhos, J. Zavašnik, A. Rečnik, A. Godelitsas, E. Chatzitheodoridis, Y. Sanakis, Spectroscopic and nanoscale characterization of blue-coloured smithsonite ($ZnCO_3$) from Lavrion historical mines (Greece), Period. di Mineral. 84 (2015) 373–388.
[4] A. Katerinopoulos, C. Solomos, P. Voudouris, Lavrion smithsonites. A mineralogical and mineral chemical study of their coloration, in: J. Mao, J. Bierlein (Eds.), Mineral deposit research: Meeting the global challenge, Springer Verlag, 2005, pp. 983–986.
[5] X. Feng, Z. Li, P. Wang, Y. Zhou, Preparation and gas-sensitivity of ultra-fine zinc-oxide powders from roasted zinc-blended, J. Mater. Sci. 40 (2005) 6597–6600.
[6] Y. Liu, J. Zhou, A. Larbot, M. Persin, Preparation and characterization of nano-zinc oxide, J. Mater. Process. Technol. 189 (2007) 379–383.
[7] K. Kakiuchi, E. Hosono, T. Kimura, H. Imai, S. Fujihara, Fabrication of mesoporous ZnO nanosheets from precursor templates grown in aqueous solutions, J. Sol–Gel Sci. Technol. 39 (2006) 63–72.
[8] I.R. Cpllins, E.S. Taylor, Non-aqueous thermal decomposition route to colloidal inorganic oxides, J. Mater. Chem. 2 (1992) 1277–1281.
[9] L. Koudelka, J. Horak, Morphology of polycrystalline ZnO and its physical properties, J. Mater. Sci. 29 (1994) 1497–1499.
[10] S.M. Mostashari, M.A. Zanjanchi, O. Baghi, Burning of a cotton fabric impregnated by synthetic zinc carbonate hydroxide as a flame retardant, Combust., Explos., Shock Waves 41 (2005) 426–429.
[11] Y.T. Pan, D.Y. Wang, One-step hydrothermal synthesis of nano zinc carbonate and its use as a promising substitute for antimony trioxide in flame retardant flexible poly (vinyl chloride), RSC Adv. 5 (2015) 27837–27843.
[12] S. Zhang, H. Fortier, J.R. Dahn, Characterization of zinc carbonate hydroxides synthesized by precipitation from zinc acetate and potassium carbonate solutions, Mater. Res. Bull. 39 (2004) 1939–1948.
[13] Abler, M.J. (1994) Dual impregnated activated carbon. US Patent 5344626.
[14] V. Sharma, S. Basak, K. Rishabh, H. Umaria, S.W. Ali, Synthesis of zinc carbonate nanoneedles, a potential flame retardant for cotton textiles, Cellulose 25 (2018) 6191–6205.
[15] Y.B. Feng, W.Q. Lu, J.Y. Cao, Z. Cai, P.F. Wang, Preparation of Nanosized Zinc Carbonate and its Kinetic Parameters of Thermal Decomposition, Chin. J. Inorg. Chem. 4 (2003) 428–432.

[16] S. Zhang, H. Fortier, J.R. Dahn, Characterization of zinc carbonate hydroxides synthesized by precipitation from zinc acetate and potassium carbonate solutions, Mater. Res. Bull. 39 (2004) 1939–1948.
[17] W. Wu, Q. Jiang, Preparation of nanocrystalline zinc carbonate and zinc oxide via solid-state reaction at room temperature, Mater. Lett. 60 (2006) 2791–2794.
[18] M. Shamsipura, S.M. Pourmortazaviab, S.S. Hajimirsadeghic, M.M. Zahedic, M. Rahimi-Nasrabadid, Facile synthesis of zinc carbonate and zinc oxide nanoparticles via direct carbonation and thermal decomposition, Ceram. Int. 39 (2013) 819–827.
[19] G.M. Sheldrick, Acta Crystallogr. Sect. A 2008 (64) (2008) 112–122.
[20] M. Isshiki, T. Irifune, K. Hirose, S. Ono, Y. Ohishi, T. Watanuki, E. Nishi-bori, M. Takata, M. Sakata, Stability of magnesite and its high-pressure form in the lowermost mantle, Nature 427 (2004) 60–63.
[21] W. Liang, Y. Yin, L. Wang, L. Chen, H. Li, A new method of preparing anhydrous magnesium carbonate ($MgCO_3$) under high pressure and its thermal property, J. Alloy. Compd. 702 (2017) 346–351.
[22] J. Gao, F. Zhu, X. Lai, R. Huang, S. Qin, D. Chen, J. Liu, L. Zheng, X. Wu, Compressibility of a natural smithsonite $ZnCO_3$ up to 50 GPa, High. Press. Res. 34 (2014) 89–99.
[23] W. Liang, L. Chen, L. Wang, Y. Yin, Z. Li, H. Li, High pressure synthesis of siderite ($FeCO_3$) and its thermal expansion coefficient, High. Temp. High. Press. 47 (2018) 153–164.
[24] H. Effenberger, K. Mereiter, J. Zemann, Crystal structure refinements of magnesite, calcite, rhodochrosite, siderite, smithonite, and dolomite, with discussion of some aspects of the stereochemistry of calcite type carbonates, Z. fur Krist. 156 (1981) 233–243.
[25] D.L. Graf, Crystallographic tables for the rhombohedral carbonates, Am. Mineral. 46 (1961) 1283–1316.
[26] W. Liang, Z. Li, Y. Yin, R. Li, L. Chen, Y. He, H. Dong, L. Dai, H. Li, Single crystal growth, characterization and high-pressure Raman spectroscopy of impurity-free magnesite ($MgCO_3$), Phys. Chem. Miner. 45 (2018) 423–434.
[27] W. Liang, Y. Yin, Z. Li, R. Li, L. Lin, Y. He, H. Dong, Z. Li, S. Yan, S. Zhai, H. Li, Single crystal growth, crystalline structure investigation and high-pressure behavior of impurity-free siderite ($FeCO_3$), Phys. Chem. Miner. 45 (2018) 831–842.
[28] W. Liang, L. Li, R. Li, Y. Yin, Z. Li, X. Liu, S. Shan, Y. He, Y. Meng, Z. Li, H. Li, Crystal structure of impurity-free rhodochrosite ($MnCO_3$) and thermal expansion properties, Phys. Chem. Miner. (2020), https://doi.org/10.1007/s00269-019-01078-2
[29] S.A. Markgraf, R.J. Reeder, High-temperature structure refinements of calcite and magnesite, Am. Mineral. 70 (1985) 590–600.
[30] R.D. Shannon, C.T. Prewitt, Effective ionic radii in oxides and fluorides, Acta Crystallogr. B25 (1969) 925–946.
[31] C.K. Huang, P.F. Kerr, Infrared study of the carbonate minerals, Am. Mineral. 45 (1960) 311–324.
[32] A. Grzechnik, P. Simon, P. Gillet, P. McMillan, An infrared study of $MgCO_3$ at high pressure, Phys. B 262 (1999) 67–73.
[33] C.G. Maier, H.K. Kelley, An equation for the presentation of high-temperature heat content data, J. Am. Chem. Soc. 54 (1932) 3243–3246.
[34] T.R. Hull, A. Witkowski, L. Hollingbery, Fire retardant action of mineral fillers, Polym. Degrad. Stab. 96 (2011) 1462–1469.
[35] V. Babrauskas, Ignition Handbook: Principles and Applications to Fire Safety Engineering, Fire Investigation, Risk Management and Forensic, Sci.: Issaqyah, Wash., Fire Sci. Publ. (2003) 1116.
[36] M.D. Walter, M.T. Wajer, Overview of Flame Retardants Including Magnesium Hydroxide, Martin. Marietta Magnes. Spec. (2010).
[37] H.D. Megaw, Crystal structures and thermal expansion, Mater. Res. Bull. 6 (1971) 1007–1018.